



Preparation of Carboxymethyl Cellulose-g-Poly(acrylamide)/Attapulgite Porous Monolith With an Eco-Friendly Pickering-MIPE Template for Ce(III) and Gd(III) Adsorption

Feng Wang^{1,2}, Yongfeng Zhu¹ and Aiqin Wang^{1*}

¹ Key Laboratory of Clay Mineral Applied Research of Gansu Province, Center of Eco-material and Green Chemistry, Lanzhou Institute of Chemical Physics, Chinese Academy of Sciences, Lanzhou, China, ² Qinzhou Key Laboratory of Biowaste Resources for Selenium-Enriched Functional Utilization, College of Petroleum and Chemical Engineering, Beibu Gulf University, Qinzhou, China

OPEN ACCESS

Edited by:

Maria Graca Rasteiro,
University of Coimbra, Portugal

Reviewed by:

Vinod Kumar Gupta,
Indian Institute of Technology
Roorkee, India
Priyanka Sharma,
Stony Brook University, United States

*Correspondence:

Aiqin Wang
aqwang@licp.cas.cn

Specialty section:

This article was submitted to
Green and Sustainable Chemistry,
a section of the journal
Frontiers in Chemistry

Received: 02 January 2020

Accepted: 15 April 2020

Published: 25 May 2020

Citation:

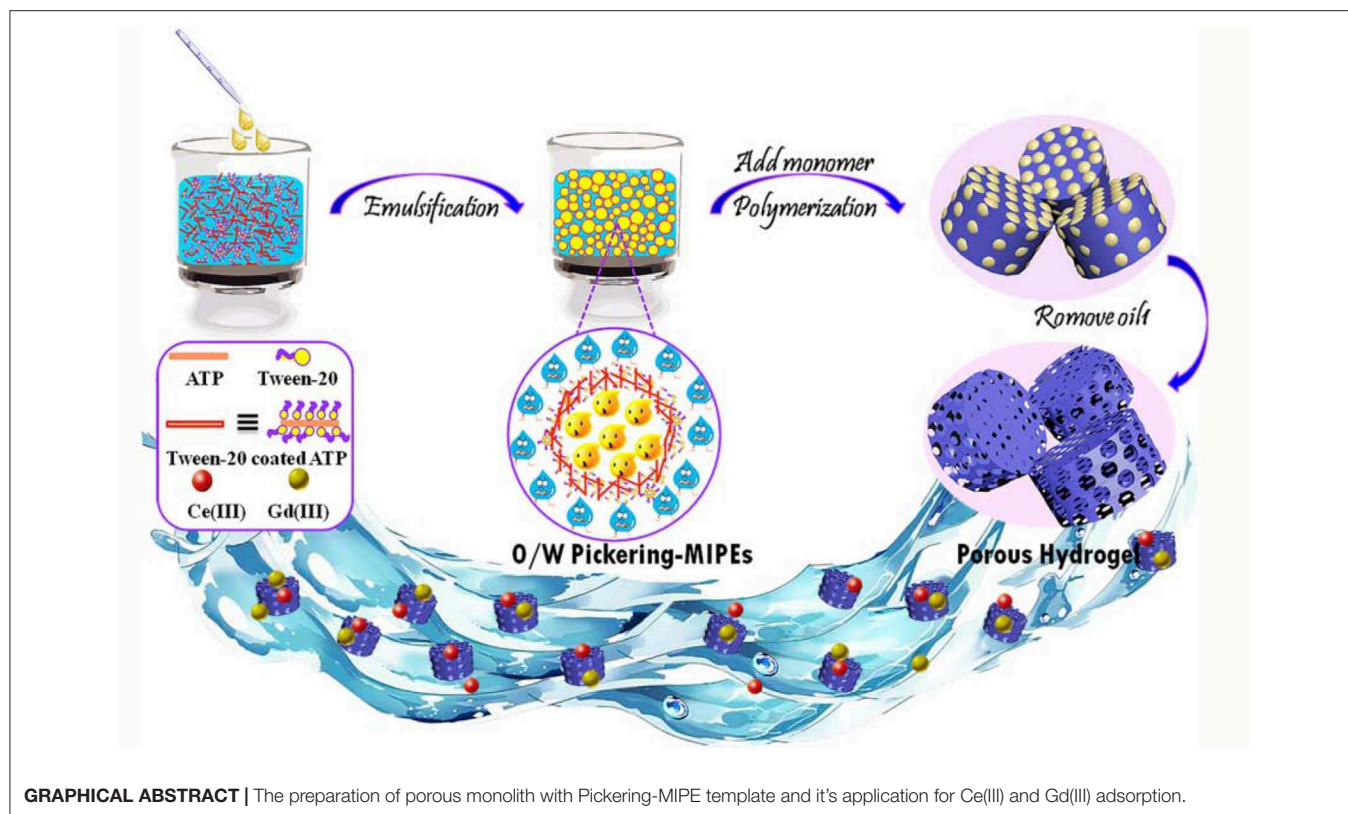
Wang F, Zhu Y and Wang A (2020)
Preparation of Carboxymethyl
Cellulose-g-
Poly(acrylamide)/Attapulgite Porous
Monolith With an Eco-Friendly
Pickering-MIPE Template for Ce(III)
and Gd(III) Adsorption.
Front. Chem. 8:398.
doi: 10.3389/fchem.2020.00398

Due to their high specific surface and metal-binding functional groups in their crosslinked polymeric networks, monolithic materials incorporating a porous structure have been considered one of the most efficient kinds of adsorbents for rare earth element recovery. Herein, a facile and novel monolithic multi-porous carboxymethyl cellulose-g-poly(acrylamide)/attapulgite was synthesized by free radical polymerization via green vegetable oil-in-water Pickering medium internal phase emulsion (O/W Pickering-MIPEs), which was synergically stabilized by attapulgite and tween-20. The homogenizer rotation speed and time were investigated to form stable Pickering-MIPEs. The effects of different types of oil phase on the formation of Pickering-MIPEs were investigated with stability tests and rheological characterization. The structure and composition of the porous material when prepared with eight kinds of vegetable oil were characterized by FTIR and SEM. The results indicate that the obtained materials, which have abundant interconnected porosity, are comparable to those fabricated with Pickering-HIPE templates. The adsorption experiment demonstrated that the prepared materials have a fast capture rate and high adsorption capacities for Ce(III) and Gd(III), respectively. The saturation adsorption capacities for Ce(III) and Gd(III) are 205.48 and 216.73 mg/g, respectively, which can be reached within 30 min. Moreover, the monolithic materials exhibit excellent regeneration ability and reusability. This work provides a feasible and eco-friendly pathway for the construction of a multi-porous adsorbent for adsorption and separation applications.

Keywords: porous materials, pickering emulsions, attapulgite, adsorption, rare earth elements

INTRODUCTION

Rare earth elements (REE) are critical components in special functional materials for industrial applications as well as in cutting-edge technology fields, such as biomedical engineering, information storage, communications, wind turbines, spaceflight, nuclear energy, and military applications (Saravanan et al., 2013; Ogata et al., 2015; Anastopoulos et al., 2016; Rajendran et al., 2016; Zhao et al., 2016, 2019; Wang et al., 2017a). China possesses more than 90% of the global



potential reserves (Survey, 2014; Ogata et al., 2015). Recently, the adsorption and recovery of REEs from aqueous solutions has become a significant issue owing to their significance (Voßenkaul et al., 2015; Alshameri et al., 2019), and many technologies are being developed to enrich REEs, including solvent extraction (Hou et al., 2013; Schirhagl, 2014), adsorption (Maranescu et al., 2019; Mondal et al., 2019; Yang et al., 2019), ion-exchange (Moldoveanu and Papangelakis, 2012; Page et al., 2019), and co-precipitation (Chatterjee et al., 2009). Among them, adsorption is considered one of the most promising methods for the removal of REEs due to its simple operation, easy separation, high efficiency, and reusability (Ogata et al., 2015; Wang et al., 2017a).

At present, various adsorbent materials have been employed to adsorb REEs from aqueous solutions including red clay (Gładysz-Płaska et al., 2014), hydrogel porous materials (Zhu et al., 2016a), carbon materials (Babu et al., 2018), silica gels (Ogata et al., 2015), marine sediments (Liatsou et al., 2015), and biopolymer microcapsules (Delrish et al., 2014). Among various adsorbents used, hydrogel porous materials are one of the most efficient types of adsorbents due to their superhydrophilic features and the metal-binding functional groups of the cross-linked polymeric networks (Ren et al., 2016). Moreover, hydrogel porous materials can be designed and tailored by various functional groups to provide them with specific properties, and the resulting functional materials are favorable for a stable adsorption process. Furthermore, the adsorption properties of adsorbents depend on their functional groups and specific surface area. A high specific surface favors the exposure of

the functional groups, improving the probability of reaction between adsorbates and adsorbents. Thus, incorporating a porous structure into adsorbents can provide a high specific surface area for adsorbents to effectively remove REE, and the porous structure also has the benefits that it reduces transmission resistance and enhances the adsorption activity of adsorbents to adsorbates (Zhu et al., 2016b). Therefore, it is indispensable to develop functional hydrogel materials with a porous structure.

The soft template method is a common method of constructing materials with ordered and disordered porous matrices (Jiaxi et al., 2015). In this method, oil-in-water Pickering high internal phase emulsions (O/W Pickering HIPEs) containing more than 74% internal phase is considered the most effective pathway for the preparation of hydrogels with well-defined porosity (Zhu et al., 2016a,b). This technology involves the polymerization of monomers in the continuous phase and the removal of the dispersed phase, which could create a solid foam material (polyHIPE) with an interconnected porous structure (Ma et al., 2014; Oh et al., 2014). Interestingly, the interconnectivity and pore structure of polyHIPEs can be easily tailored by varying the parameters of O/W Pickering HIPEs (Ikem et al., 2010a; Ye et al., 2013). Therefore, large numbers of adsorbents with interconnected structures have been successfully prepared by using O/W Pickering HIPEs (Yi et al., 2016), and the as-prepared adsorbents exhibited enhanced adsorption capacity to model pollutants due to abundant porosity and high permeability (Zhang et al., 2016).

However, the O/W Pickering HIPEs have some obvious drawbacks. For example, this method often requires more than 74% of an organic solvent (such as liquid paraffin, toluene, *p*-xylene, or *n*-hexane) as the dispersion phase, and needing a large amount of these organic solvents greatly increases the preparation cost; in addition, these are harmful to the environment and human health. It is thus desirable to decrease the oil phase fraction and substitute poisonous organic solvent with an eco-friendly oil phase. Compared with Pickering-HIPEs, the formation of Pickering-medium internal phase emulsions (Pickering-MIPEs) requires less of the dispersion phase. Therefore, in this research, porous materials with medium internal phase emulsions have been fabricated by using cheap vegetable oil as the dispersion phase. In addition, particles with appropriate wettability are a necessary condition for preparing a stable O/W Pickering emulsion. In order to achieve the necessary wettability, solid particles [such as inorganic particles (Gudarzi and Sharif, 2011), polymer micelles (Yang et al., 2016), colloidal particles (Gautier et al., 2007), and carbon materials (Sullivan and Kilpatrick, 2002)] usually need to be modified by chemical and physical processes, but it is inevitable that this will result in waste energy and an increase of production cost. For these reasons, natural particles that require no further modification are considered excellent stabilizers for the construction of interconnected porous materials. Due to their plentiful hydroxyl groups and negative charge, clay minerals are highly hydrophilic and present the potential for use in the formation of an O/W emulsion as stable particles without any further modification.

In this study, natural attapulgite (ATP) was employed as the stable particle, tween-20 (T-20) served as the co-stabilizer, and vegetable oil was selected as the disperse phase to form eco-friendly O/W Pickering-MIPEs for the construction of porous materials. In order to form stable Pickering-MIPEs, the effects of the type of oil phase, the homogenizer rotation speed, and time on the formation of Pickering-MIPEs were investigated. Sodium carboxymethyl cellulose (CMC) has two different end groups: one has a chemically reducing functionality (a hemiacetal unit), and the other has a pendant hydroxyl group that can be used to react with other monomers (Klemm et al., 2005). Moreover, the groups on CMC were found to be effective for the removal of metal ions from water (Sharma et al., 2017; Klemm et al., 2018). Thus, in this research, CMC was employed as the grafting backbone onto which to graft acrylamide (AM), which was used as the functional monomer due to its ability to combine with metals and its reactivity. The adsorption properties of the obtained porous cellulose-*g*-poly(acrylamide)/attapulgite materials for Ce(III) and Gd(III) from aqueous solution was also studied.

EXPERIMENTAL SECTION

Materials

CMC (CP, viscosity: 300-800 mpa·s) and AM (CP) were purchased from Shanpu Chemical Factory (Shanghai, China) and used without further treatment. Ammonium persulfate (APS, AR), *N,N,N',N'*-tetramethyl ethylenediamine (TMEDA, AR), Methyl violet (MV), and Methylene blue (MB) were

provided by Sinopharm Chemical Reagent Co., Ltd. (Shanghai, China). ATP was obtained from Huangnishan Mine in Xuyi county, Jiangsu province, China, and then ground and passed through a 200-mesh sieve. *N,N'*-methylenebisacrylamide (MBA, CP) was received from Yuanfan Vegetable Additives (Shanghai, China). T-20 (AR) was received from BASF Corporation. 3A molecular sieve 103 was obtained from Molsion Molecular Sieve Co., Ltd. (Shanghai, China). Linseed oil was purchased from Yongfan Trading Co. (Lanzhou, China). Colza oil and soybean oil were purchased from Yihaijiali Arawana Edible Oil Co., China. Peanut oil, sunflower oil, olive oil, and sesame oil were obtained from Shandong Luhua Group Co., Ltd. China. Corn oil was purchased from Cofco Food Marketing Co., Ltd. China. Other reagents were all of analytical grade, and all solutions were prepared with deionized water.

Preparation of Pickering-MIPEs

T-20 (0.2 g) and ATP (0.5 g) were dissolved into 10 mL deionized water under 3,000 rpm stirring for 1 min, and then various vegetable oils (10 mL) were added into the mixed suspension separately and emulsified with a GJD-B12K homogenizer at certain rpm values for a designed time to form Pickering MIPEs. The type of emulsion was detected by the pendant-drop method with deionized water and *p*-xylene. The emulsion droplet could disperse into deionized water but remained round in *p*-xylene, indicating that the as-prepared Pickering-MIPEs were O/W emulsions. The feed composition of reactants, the codes of the emulsions, and the corresponding droplet diameters are listed in **Table 1**.

Preparation of Porous CMC-*g*-PAM Monolith

The stable Pickering-MIPEs containing 0.1 g CMC, 0.31 g MBA, 2% T-20, and 5% ATP were prepared by first dissolving CMC and MBA in the continuous phase. After the emulsion was obtained, 1.42 g (2 mmol) AM, 91 mg APS, and 0.1 mL of TMEDA were added into it with rapid stirring for 1 min, and then the prepared mixture was transferred into test tubes, sealed, and immersed in a 65°C water bath for 12 h to complete the polymerization reaction. After that, the porous polymers were sectioned and washed with acetone via Soxhlet extraction for 10 h. In order to activate the porous polymers, they were immersed in 0.5 M NaOH aqueous alcohol solution (V/V, 3/7) for 24 h to transform amide groups into carboxyl groups. The redundant NaOH and undesirable residues were washed away with a water/ethanol ($V_{\text{water}}/V_{\text{alcohol}} = 3/7$) solvent, repeatedly, and then the monolithic hydrogels were dehydrated with 3A molecular sieve in absolute ethanol and then dried at 60°C in a vacuum for 8 h. The feed composition of the reactants, the codes of the porous monoliths, and the corresponding pore diameters are also summarized in **Table 1**. Photographs of the materials are shown in **Figure 4**.

Characterization

FTIR spectra were obtained by a Nicolet NEXUS FTIR spectrometer (U.S.A.) in the 4,000–400 cm^{-1} wavenumber region after the samples had been prepared as KBr pellets. The morphologies of the porous monoliths were characterized using

TABLE 1 | Feed composition of Pickering MIPE formulations and porous CMC-*g*-PAM/ATP monoliths and their corresponding average droplet and pore sizes.

Emulsion	Speed (rpm)	Time (min)	Emulsion	Speed (rpm)	Time (min)	Oil
ES-4000	4,000	10	ES-12000	12,000	10	Linseed oil
ES-6000	6,000	10	ET-1	10,000	1	Linseed oil
ES-8000	8,000	10	ET-3	10,000	3	Linseed oil
ES-4000	4,000	10	ET-5	10,000	5	Linseed oil
ES-10000	10,000	10	ET-7	10,000	7	Linseed oil
ES-11000	11,000	10	ET-9	10,000	9	Linseed oil

Emulsion	D _E (μm) ^a	Materials	D _M (μm) ^b	Speed (rpm)	Time (min)	Oil
E1	2.54	S1	2.35	10,000	7	Linseed oil
E2	2.48	S2	2.29	10,000	7	Colza oil
E3	2.57	S3	2.39	10,000	7	Peanut oil
E4	2.49	S4	2.32	10,000	7	Sunflower oil
E5	2.52	S5	2.27	10,000	7	Soybean oil
E6	2.58	S6	2.31	10,000	7	Corn oil
E7	2.55	S7	2.28	10,000	7	Olive oil
E8	2.43	S8	2.24	10,000	7	Sesame oil

^a Average diameter of emulsion droplets.

^b Average pore diameter of materials.

a field emission scanning electron microscope (SEM, JSM-6701F, JEOL, Japan) after being coated with gold film. The average pore diameter was obtained by measuring 100 pores using Image-Pro Plus 6.0 software. A Leica DM1000 digital biological microscope equipped with a built-in camera was used to record optical microscopy images of the Pickering-MIPES.

Evaluation of Adsorption Performance

Working solutions containing different concentrations of Ce(III) and Gd(III) were prepared by diluting the stock solution of Ce(NO₃)₃ or Gd(NO₃)₃ using deionized water. The monolithic adsorbents were ground into granular particles with a particle size in the range of 12–40 mesh to conduct the adsorption experiments.

The adsorption process was performed by immersing 20 mg of adsorbent in 25 mL Ce(III) and Gd(III) solutions and shaking with a thermostatic shaker (THZ-98A) at 120 rpm and 30°C for a given time to reach adsorption equilibrium. After that, the monolith was separated from the solution, and the absorbance of solutions was measured by a UV-visible spectrophotometer (UV-3010, HITACHI, Japan) to measure the concentrations of Ce(III) and Gd(III) in the solution. The complexing agents used in this case are chlorophosphonazo and azo arsine for Ce(III) and Cd(III), respectively. The maximum absorbance wavelengths are 666 nm for Ce(III) and 656 nm for Gd(III). The adsorption capacities of the porous monolith for Ce(III) and Gd(III) were calculated according to Equation (1):

$$q_e = (C_0 - C_e) \times 0.025 / m \quad (1)$$

where, q_e (mg/g) is the amount of Ce(III) or Gd(III) adsorbed by per unit mass of adsorbent and C_0 and C_e (mg/L) are the concentrations of Ce(III) or Gd(III) before and after adsorption,

respectively, 0.025 (L) is the volume of Ce(III) or Gd(III) solution used for adsorption, and m (mg) is the mass of adsorbent.

During the experiment, the pH of the solution was adjusted to the required value with 0.1 mol/L HCl or NaOH solutions. The influence of pH value on the adsorption capacities of the porous monolith (S2) was evaluated in rare earth metal solutions with an initial concentration of 200 mg/L and pH values from 1 to 7. The effect of initial concentration on the adsorption capacities of the porous monolith was investigated by adding adsorbent (S2) into solutions with concentrations in the range of 100–400 mg/L for 1 h at the original pH of the solution. The adsorption kinetics was determined by ranging the adsorption duration from 5 to 120 min at the original pH of the solution and with a solution concentration of 200 mg/L. All adsorption experiments were repeated thrice to obtain the average value.

Desorption experiments were conducted to show the recyclability of the prepared porous hydrogel. Typically, 20 mg of the adsorbent (S2) was fully contacted with 25 mL 200 mg/L at 120 rpm and 30°C for 1 h to attain saturation adsorption. The metal-loaded adsorbent was then soaked in 30 mL HCl (0.5 mol/L) solution for 2 h to desorb, and then soaked with 0.5 mol/L NaOH solution and fully washed to neutral with deionized water to activate, after which the adsorbent was used for another adsorption process. The adsorption-desorption cycle was repeated five times to evaluate the reusability of the monolith.

RESULTS AND DISCUSSION

Preparation of Pickering-MIPES Stabilized by ATP and T-20

The eco-friendly O/W Pickering MIPES were formed by using vegetable oil as the dispersion phase and ATP and T-20 as the

stabilizer after vigorous stirring for the designed time. During the stirring progress, T-20 first coated the surface of the ATP and then coated ATP nanorods synergistically with other free surfactants at the oil–water interface, acting as a barrier to prevent the coalescence of oil droplets and to generate a stable emulsion, as shown in **Scheme 1**.

The Effects of Emulsification Speed and Time

The homogenizer rotation speed and time are important factors for obtaining a homogenous emulsion (Colla et al., 2006), and thus the effects of the stirring velocity and time were investigated in this case. The experiment details are listed in **Table 1**; all the emulsions were stabilized by 5% ATP and 2% T-20. After preparation, the emulsion was kept for a month to observe its stability. As shown in **Figure 1**, the homogenizer rotation speed had a greater effect on the stability of emulsions compared with emulsification duration (**Figure 1A**). As the emulsification velocity and shear stress increased, the energy of the emulsion systems also increased to reduce the system energy, and the droplet size of emulsions largely reduced. The increase in the emulsification velocity expanded the contact area of the aqueous and oil phases, allowing more efficient dispersal and breakup of oil droplets in the emulsion and thus greatly enhancing the stability of emulsions. It is worth noting that an excessive emulsification speed introduced a large amount of bubbles into the emulsion. According to **Figure 1**, the volume of emulsion remained the same after the velocity reached 10,000 rpm, and thus 10,000 rpm was selected for the evaluation of the effect of emulsification duration.

At the same emulsification speed, an increase in the emulsification duration also helped to form a stabilized emulsion. Sufficient emulsification time could enhance the dispersion of the emulsion, decrease the diameter and wall thickness of droplets,

and also increase the amount of droplets. However, collisions between droplets due to the mechanical agitation led to their aggregation and the formation of foam at the critical time, and

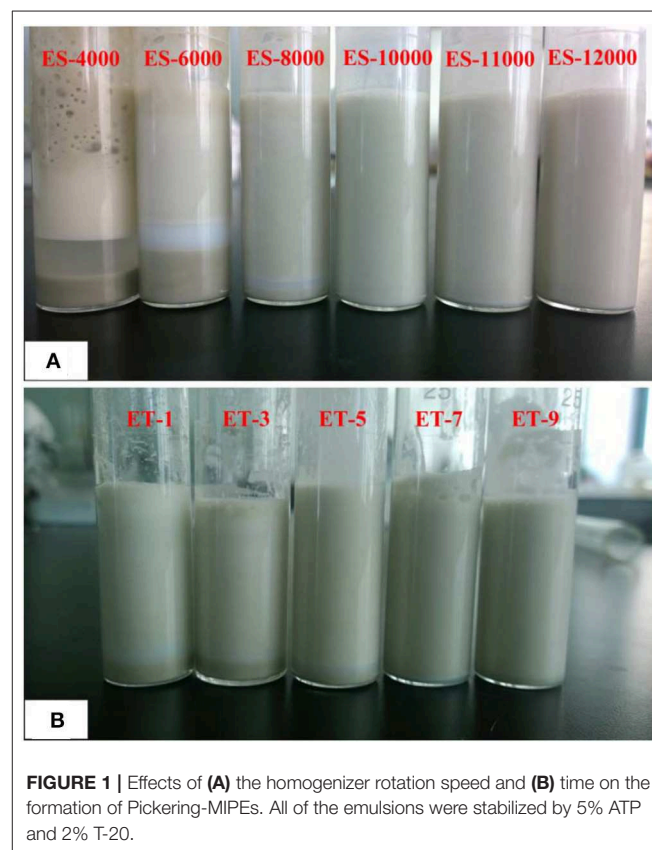
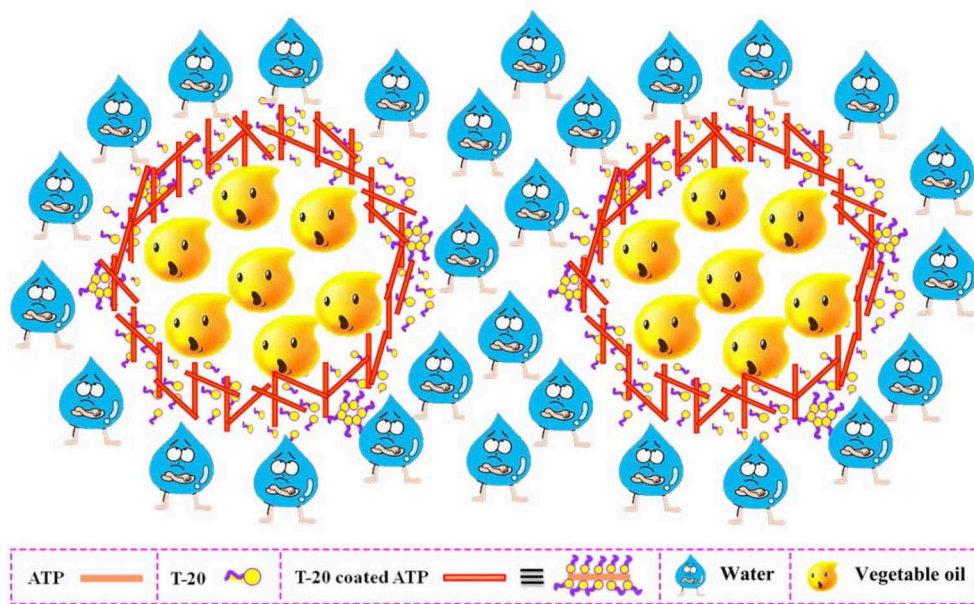


FIGURE 1 | Effects of (A) the homogenizer rotation speed and (B) time on the formation of Pickering-MIPes. All of the emulsions were stabilized by 5% ATP and 2% T-20.



SCHEME 1 | Formation of O/W Pickering-MIPes stabilized by ATP and T-20.

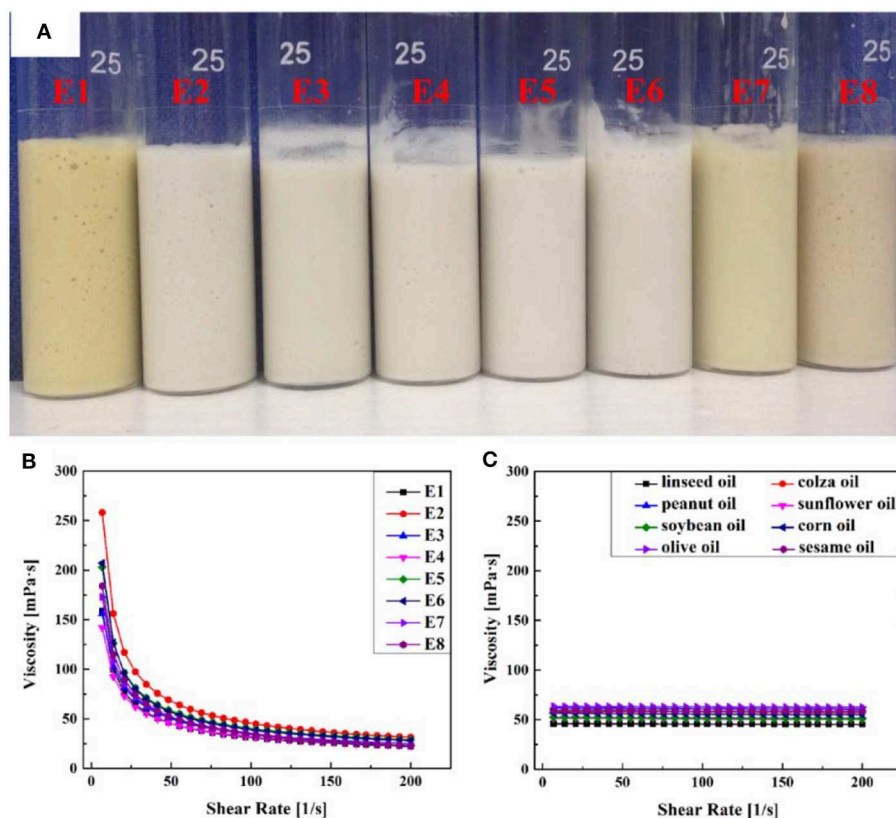


FIGURE 2 | (A) Digital photographs of Pickering emulsions prepared with various vegetable oils. Rheological characterization of (B) the corresponding Pickering emulsions and (C) the different vegetable oils.

thus it was essential to find the appropriate duration for an emulsion process. As shown in **Figure 1B**, stabilized emulsions were obtained after being stirred for 7 min, and thus the optimal duration of the emulsion process was 7 min.

The Effect of the Oil Phase

The effect of eight types of vegetable oil on the emulsions was also studied. Digital photographs and rheological characterization of Pickering emulsions with various vegetable oils are shown in **Figure 2**. As depicted in **Figure 2A**, the emulsions prepared with eight kinds of vegetable oils maintained good stability for at least 1 month after being agitated at 10,000 rpm for 7 min, and no oil–water separation was observed. The different colors of the eight emulsions might be attributable to the different original colors of the oil phases. A sliding test indicated that the emulsions could stay on a vertical glass tube without any flow, which suggested that the emulsions formed were typical gel emulsions and that the oil drops were closely packed, which was also verified from their optical micrographs (**Figure 3**). It was also confirmed that the increase in the viscosity of emulsions could inhibit the coalescence of emulsion droplets and improve the stability of emulsion (Ikem et al., 2008). Therefore, a stress-controlled rheometer was used to evaluate the viscosity of the prepared Pickering emulsions. The rheological characterization reveals that there was no significant difference in the viscosity

of the eight emulsions (**Figure 2B**) and the viscosity of the corresponding vegetable oils (**Figure 2C**).

The optical microscope images of the obtained emulsions are shown in **Figure 3**. It was found that the droplets of all eight emulsions accumulated together compactly and that the average droplet diameters of the eight emulsion droplets were almost the same (**Table 1**). The lack of visible difference between the emulsion diameters might be another important reason for the similar viscosity of the emulsions. The above experimental results proved that type of oil did not have a significant influence on the emulsion, and thus all vegetable oils used in this research were suitable for preparing a stable O/W Pickering emulsion.

Formation of CMC-g-PAM/ATP

The porous monoliths were obtained by free radical polymerization of the reactants in the continuous phase using APS as the initiator. The decomposition of APS at 65°C induced the CMC to generate macro-radicals, and the monomer of AM was grafted onto CMC. The three-dimensional net structure polymer was then formed in the presence of the crosslinker MBA. After the reaction was finished, the products were Soxhlet extracted with acetone immediately for 10 h to remove the oil phase, and monoliths with porous morphology were observed (**Figure 4**). This suggested that the incorporation of appropriate ATP and a low dosage of T-20 as a Pickering stabilizer was

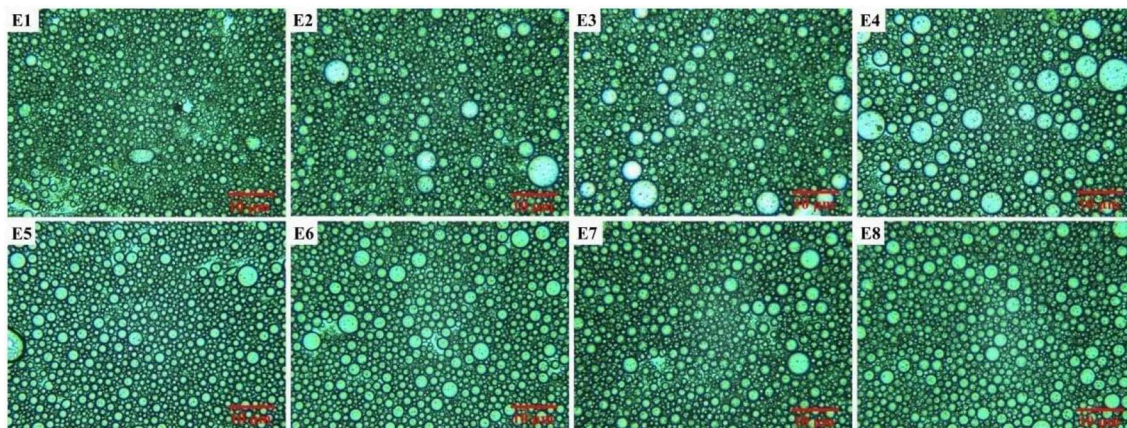


FIGURE 3 | Optical microscope images of Pickering emulsions prepared with different oil phases.

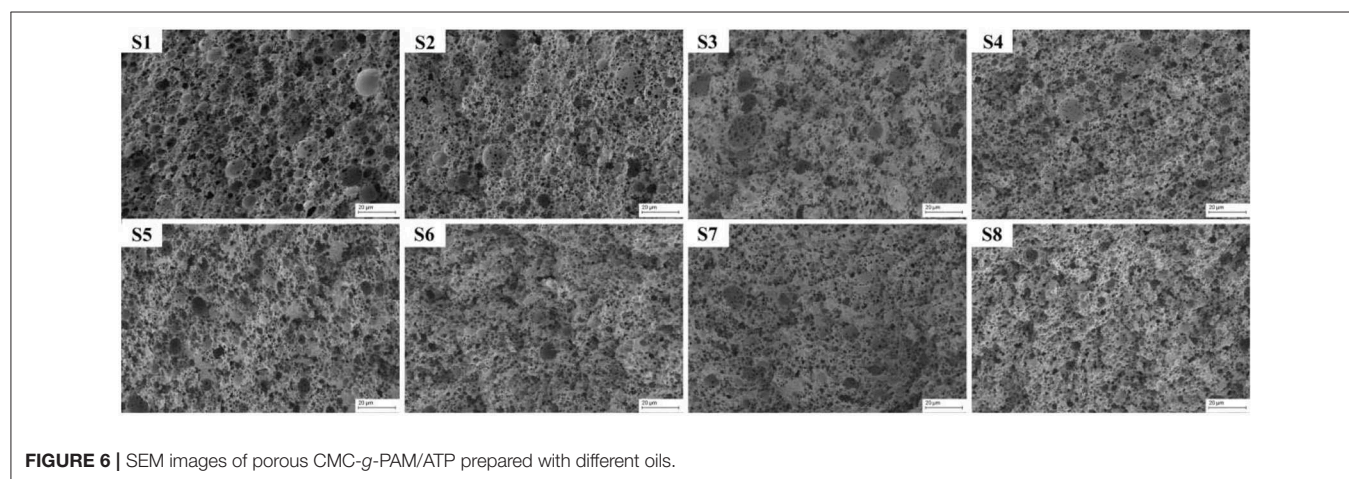
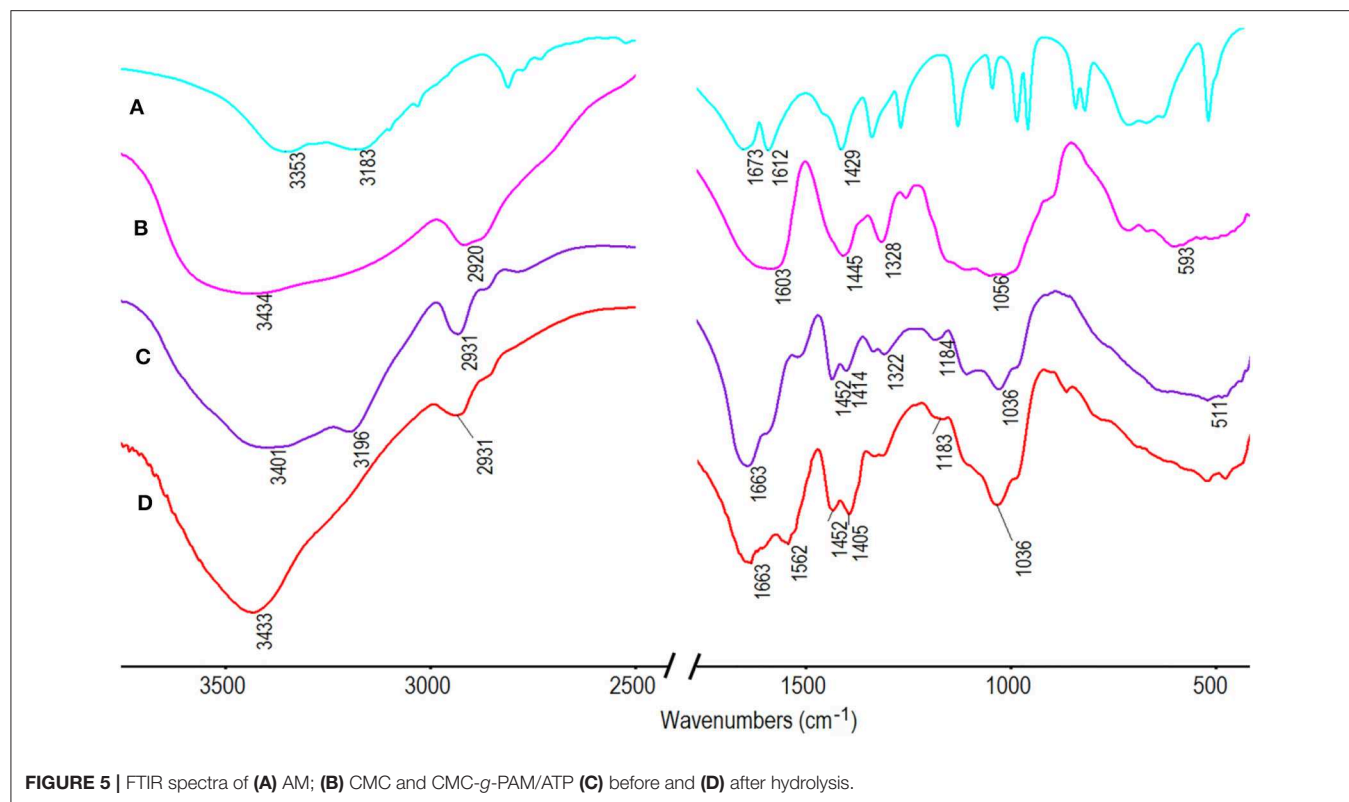


FIGURE 4 | Digital photographs of the porous CMC-g-PAM/ATP hydrogels prepared through the use of Pickering-MIPes with various vegetable oils.

successful in forming a porous structure inside hydrogels during the polymerization and post-treatment. The elution of the oil phase contributed to the formation of macropores, while the thinner monomer layer between neighboring droplets resulted in open pore throats between neighboring macropores (Xu et al., 2016; Wang et al., 2017b).

FTIR spectra of AM, CMC, and CMC-g-PAM/ATP before and after hydrolysis are compared in **Figure 5** to confirm the formation of the target porous adsorbent. The absorption band of CMC at $3,434\text{ cm}^{-1}$ (the OH stretching vibration of CMC) overlapped with the O-H stretching vibrations of the (Fe, Mg) O-H and (Al, Mg) O-H of ATP (Wang et al., 2015) after the reaction and appeared at $3,401\text{ cm}^{-1}$ in the spectrum in **Figure 5C**. The band of AM at $1,673\text{ cm}^{-1}$ assigned to C=O stretching vibration and the band of CMC at $1,603\text{ cm}^{-1}$ attributed to asymmetric stretching vibration of carboxylate overlapped and appeared at $1,663\text{ cm}^{-1}$ in

the spectrum of CMC-g-PAM/ATP (**Figure 5C**), indicating successful grafting of the AM monomer onto the CMC (Xiao et al., 2015). The absorption band at $1,036\text{ cm}^{-1}$ (**Figure 5C**) was assigned to the Si-O-Si asymmetric stretching vibration, indicating the existence of ATP in the porous monolith. After hydrolysis, the characteristic absorption at $3,196\text{ cm}^{-1}$ (**Figure 5C**) ascribed to -NH_2 groups disappeared, and the O-H stretching vibration presented an obvious blue shift and appeared at $3,433\text{ cm}^{-1}$. Furthermore, the characteristic absorption band of the C=O in amide at $1,663\text{ cm}^{-1}$ weakened, and the absorption peaks at $1,562$ and $1,405\text{ cm}^{-1}$, which were assigned to asymmetric and symmetric stretching vibration of -COO^- groups, appeared after hydrolysis, indicating that the amide groups were successfully converted into carboxyl groups (Ghorai et al., 2014). Moreover, the absorption band of Si-O-Si asymmetric stretching vibration of ATP persisted after hydrolysis.



The surface morphologies of the porous materials prepared by Pickering MIPs with different vegetable oils are exhibited in **Figure 6**. The SEM images of eight porous materials presented similar surface morphologies, which indicated that the effect of the type of vegetable oil on the pore structure was almost negligible. All of the materials exhibit interconnected and distinct hierarchical porous structures, with both macropores and pore throats clearly visible in their SEM images. The statistical data in **Table 1** indicated that the average macropore sizes of the eight materials were relatively uniform about 2.3 μm , which was consistent with the droplet size of the corresponding emulsions, indicating that there was no structural shrinkage during the

polymerization and post-treatment process. In general, the macropore size of materials prepared by the high internal phase emulsion template method is about 100–700 μm (Ikem et al., 2010b). By contrast, the macropore diameter of materials prepared in this paper was greatly reduced, which could effectively improve the specific surface area of the materials.

Adsorption Properties of CMC-g-PAM/ATP for Ce(III) and Gd(III)

The adsorption properties of CMC-g-PAM/ATP for Ce(III) and Gd(III) were next evaluated. As shown in **Figure 7A**, all adsorbents exhibited almost the same adsorption efficiency, with

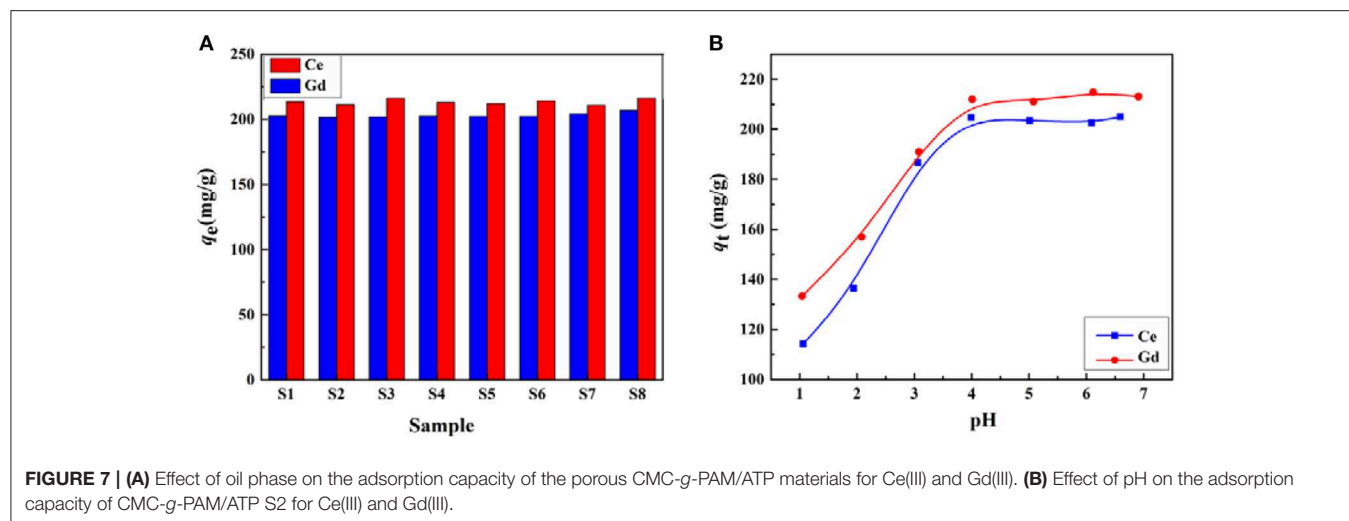


FIGURE 7 | (A) Effect of oil phase on the adsorption capacity of the porous CMC-g-PAM/ATP materials for Ce(III) and Gd(III). **(B)** Effect of pH on the adsorption capacity of CMC-g-PAM/ATP S2 for Ce(III) and Gd(III).

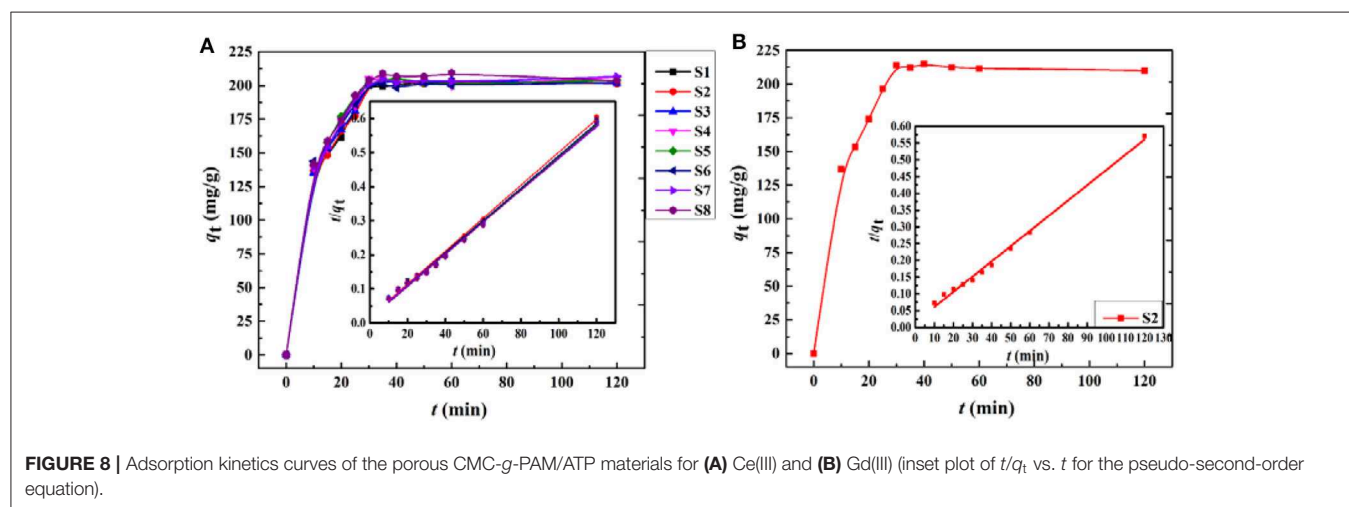


FIGURE 8 | Adsorption kinetics curves of the porous CMC-g-PAM/ATP materials for **(A)** Ce(III) and **(B)** Gd(III) (inset plot of t/q_t vs. t for the pseudo-second-order equation).

adsorption capacities for Ce(III) and Gd(III) of around 205 and 216 mg/g, respectively. The similar adsorption properties for Ce(III) and Gd(III) might be due to the similar chemical compositions and porous structures of the as-prepared porous monoliths. The results indicate that the Pickering MIPES prepared in this study exhibit wide applicability and can be prepared from various kinds of vegetable oils.

Effect of pH on Adsorption of Ce(III) and Gd(III)

To determine the effects of pH on adsorption of Ce(III) and Gd(III), the adsorption experiments were carried out at different pH values; the results are shown in **Figure 7B**. When the pH value was higher than 7.0, the metal ions involved were hydrolyzed, so pH values from 1 to 7 were selected for the tests. The adsorption properties of monoliths were highly pH-dependent, and the adsorption capacity was mainly governed by the number of charged functional groups on the backbone. It was clear that the adsorption capacity of the CMC-g-PAM/ATP to Ce(III) and Gd(III) presented a remarkable increase with an increase in pH up to 4.0, above which the adsorption capacity

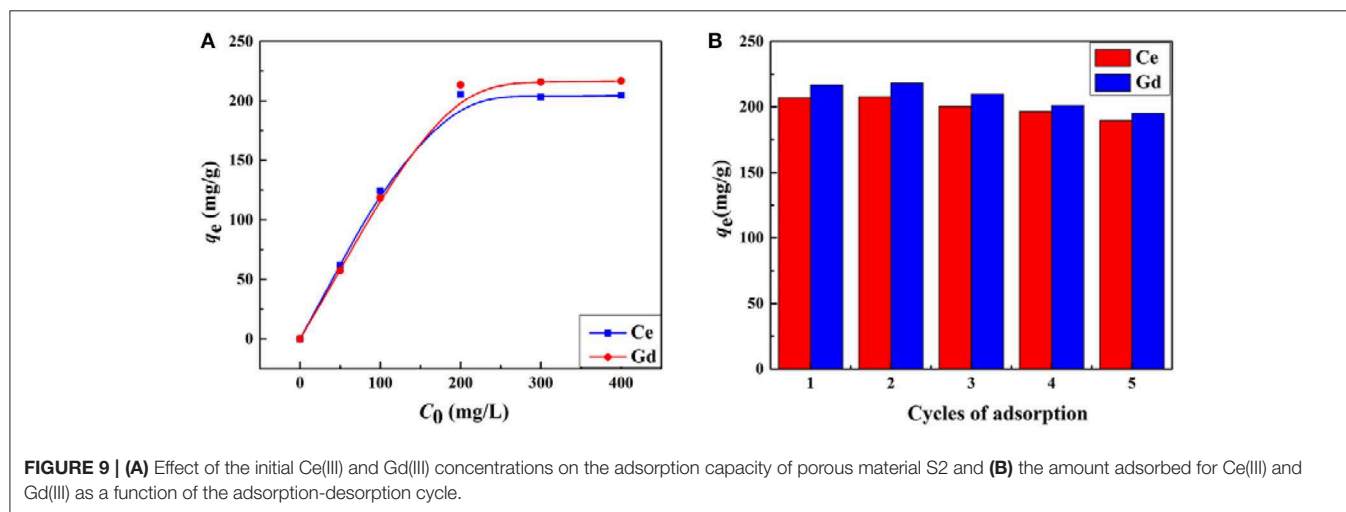
became stable. This phenomenon might be attributable to the protonation of $-\text{COO}^-$ under the strongly acidic conditions (Wang W. et al., 2013). The protonation would reduce the complexation ability of the adsorbent with metal ions (Ijagbemi et al., 2010). With the increase in pH value, a part of the $-\text{COOH}$ groups transformed into $-\text{COO}^-$ groups, which had stronger complexing ability with metal ions than $-\text{COOH}$, so the higher pH value facilitated the adsorption capacity of the adsorbents. As the initial pH increased from 4.0 to 7.0, all the carboxylic groups of the adsorbent had been dissociated and charged, and thus a constant adsorption capacity was observed.

Effect of Contact Time on Adsorption of Ce(III) and Gd(III)

The adsorption kinetics of the adsorbent is a significant parameter for practical application. The kinetic adsorption curves of the porous monoliths with different oil phases are shown in **Figure 8**. The figure demonstrates that the adsorption rate of the porous monoliths for the metal ions increased remarkably in the first 30 min and that the degree of adsorption

TABLE 2 | Adsorption kinetic parameters for adsorption of Ce(III) and Gd(III) onto CMC-g-PAM/ATP.

Sample	Pseudo-first-order equation			Pseudo-second-order equation			$q_{e,exp}$ (mg/g)	Metal
	$q_{e,cal}$ (mg/g)	$K_1 \times 10^{-2}$ (min^{-1})	R^2	$q_{e,cal}$ (mg/g)	$K_2 \times 10^{-3}$ (g/mg min)	R^2		
S1	45.99	04.34	0.4823	212.28	1.19	0.9959	203.58	Ce(III)
S2	36.84	3.29	0.2594	207.12	1.30	0.9973	205.61	Ce(III)
S3	37.91	3.73	0.3651	211.15	1.35	0.9971	204.37	Ce(III)
S3	91.89	7.39	0.4706	214.61	1.22	0.9975	206.17	Ce(III)
S5	33.72	3.64	0.3197	211.40	1.57	0.9977	205.73	Ce(III)
S6	46.79	3.14	0.5010	210.46	1.42	0.9977	202.56	Ce(III)
S7	123.97	8.35	0.7361	215.43	1.23	0.9975	206.65	Ce(III)
S8	23.99	2.85	0.0633	211.93	1.78	0.9958	208.94	Ce(III)
S2	38.93	3.02	0.2651	220.26	1.33	0.9943	215.15	Gd(III)



reached a steady state after 30 min. The adsorption curves also showed that the adsorption rates of the eight materials for Ce(III) were basically consistent, and thus only S2 was selected as a representative to evaluate the adsorption rate for Gd(III). The adsorption tendency for Gd(III) showed that S2 also had a fast adsorption rate for Gd(III) and reached adsorption equilibrium by 30 min, which was similar to the adsorption behavior for Ce(III). The fast adsorption rate profited from the interconnected pores of the materials, which efficiently reduced the mass transfer resistance and exposed more binding sites for metal ions, thus improving the accessibility of metal ions to the adsorbent (Gupta et al., 2014).

In order to examine the potential rate-controlling steps during the adsorption process, pseudo-first-order (Equation 2) and pseudo-second-order (Equation 3) models (Ghaedi et al., 2015) were tested to fit the experimental data. The equations of the kinetic models are expressed as follows:

$$\text{Log}(q_e - q_t) = \text{log}q_e - (k_1/2.303)t \quad (2)$$

$$t/q_t = 1/(k_2 \times q_e^2) + t/q_e \quad (3)$$

where q_t is the adsorption capacity for Ce(III) or Gd(III) at time t , and q_e is the equilibrium adsorption capacity. k_1 (min^{-1}) and k_2 [$\text{g}/(\text{mg min})$] are the adsorption rate constants of the pseudo-first-order and pseudo-second-order models, respectively. As shown in **Table 2**, the adsorption of Ce(III) and Gd(III) onto the porous monolith adsorbents followed the pseudo-second-order model rather than pseudo-first-order model by comparison with their linear correlation coefficients (R^2). In addition, the calculated q_e values ($q_{e,cal}$) with the pseudo-second-order kinetic model were much closer to the experimental values ($q_{e,exp}$). This suggested that the adsorptions of the porous monoliths for Ce(III) and Gd(III) were probably controlled by a chemical adsorption process (Zhou S. et al., 2014; Zhou Y. et al., 2014).

Effect of Initial Concentration on Adsorption of Ce(III) and Gd(III)

The influence of the initial concentrations of metal ions on the adsorption capacity of the materials was investigated in the range of 50–400 mg/L. As shown in **Figure 9A**, the saturation adsorptions of the porous monolith (S2) for Ce(III) and Gd(III) were reached when the initial concentration increased to 200 mg/L, and then the increasing trend flattened. The maximum

TABLE 3 | Adsorption isotherm constants of Ce(III) and Gd(III) onto CMC-g-PAM/ATP.

Metal	Langmuir model				Freundlich model		
	$q_{e, \text{exp}}$ (mg/g)	q_m (mg/g)	b (L/mg)	R^2	K	n	R^2
Ce ³⁺	205.48	205.56	0.7734	0.9999	86.68	5.57	0.6563
Gd ³⁺	216.73	224.52	0.1489	0.9973	56.73	3.58	0.6148

TABLE 4 | Comparison of adsorption capacities (q_m , mg/g) and rates (T, min) of various adsorbents for Ce(III) and Gd(III).

Adsorbent	Ce(III)		Gd(III)		References
	q_m (mg/g)	T (min)	q_m (mg/g)	T (min)	
Zn/Al LDH-intercalated cellulose	96.25	10	–	–	Iftekhhar et al., 2017
Corn style	180.20	240	–	–	Jaya et al., 2014
Prawn carapace	218.30	360	–	–	Jaya et al., 2014
Mesoporous conjugate adsorbent	192.31	25	–	–	Awual et al., 2013
Loofah fiber-g-acrylic acid (LF-AA)	527.5	120	–	–	Liu et al., 2017
Wheat straw	298.60	100	–	–	Zhou et al., 2016
Poly(allylamine)/silica composite	111.8	60	–	–	Zhou S. et al., 2014
Colloidal graphene oxide	–	–	286.86	30	Chen et al., 2014
1,2-HOPO-SAMMS	–	–	80	30	Yantasee et al., 2010
Cross-linked polyvinyl amidoxime fiber	–	–	14.83	150	Yang et al., 2018
By-pass cement	–	–	100	–	Ali et al., 2011
Polyethyleneglycol (phosphomolybdate and tungstate)	–	–	57	–	Zhang et al., 2009
CTS-g-(AA-co-SS)/ISC hydrogel	174.05	20	223.79	20	Wang et al., 2017a
Kenaf cellulose-based poly(hydroxamic acid)	245	–	220	–	Rahman et al., 2017
CMC-g-PAM/ATP	205.48	30	216.73	30	This study

adsorption capacities for Ce(III) and Gd(III) were 205.48 and 216.73 mg/g, respectively. As the concentrations of Ce(III) and Gd(III) increased, the inside and outside concentration gradient of the material increased, thus strengthening the adsorption driving force, which was beneficial for Ce(III) and Gd(III) to overcome the transfer resistance and spread to the interior of the 3D network. Once all the adsorption sites of the adsorbent were completely occupied by metals ions, adsorption equilibrium was reached.

The adsorption process was simulated by the Langmuir (Equation 4) and Freundlich (Equation 5) isotherm models (Mittal et al., 2010; Chen et al., 2019). The respective equations are as follows.

$$\frac{C_e}{q_e} = \frac{1}{q_m b} + \frac{C_e}{q_m} \quad (4)$$

$$\log q_e = \log K + (1/n) \log C_e \quad (5)$$

where C_e (mg/L) represents the equilibrium concentration of metal ions, and q_e and q_m are the adsorption capacity (mg/g) of adsorbent at any time and in equilibrium state (mg/g), respectively. b (L/mg) is the Langmuir constant related to the affinity of binding sites (mg), which can be calculated by the slope ($1/q_m$) and intercept ($1/q_m \times b$) of plot (C_e/q_e) vs. C_e . K is a Freundlich constant related to adsorption capacity, and n

is a dimensionless constant representing an index of adsorption intensity or surface heterogeneity. K and n can also be calculated by the slope ($1/n$) and intercept ($\log K$) of plot ($\log q_e$) vs. $\log C_e$.

The related isotherm parameters and correlation coefficients (R^2) were calculated and are summarized in **Table 3**. The fitting results proved that the relevant parameters of the Langmuir isothermal model (Ce(III): 0.9999, Gd(III): 0.9973) were much higher than those of the Freundlich isothermal model (Ce(III): 0.6563, Gd(III): 0.6148). The maximum adsorption capacities for Ce(III) and Gd(III) calculated by the Langmuir model were 205.56 and 224.52 mg/g, respectively, which were very close to the experimental values of 205.48 and 216.73 mg/g, respectively. The above analysis indicates that the Langmuir model was suitable for fitting the adsorption process of rare earth metals onto the adsorbent, suggesting that the binding sites were evenly distributed on the adsorbent surface, as these binding sites exhibited the same affinity for adsorption as a single molecular layer (Wang J. et al., 2013). Moreover, it can also be seen from **Table 4** that the saturated adsorption capacities of the macroporous monolith prepared in this study were much higher than those of the adsorbents reported previously, and so was the adsorption rate.

Reusability of CMC-g-PAM/ATP for Ce(III) and Gd(III)

Reusability is an important parameter for evaluating the properties of an adsorbent. In this section, S2 was selected

to investigate the regeneration performance. Given that the prepared porous adsorbent contains a large number of carboxyl groups, which are sensitive to H^+ , hydrochloric acid (0.5 mol/L) was selected as the eluent for desorption of Ce(III) and Gd(III) from CMC-g-PAM/ATP after adsorption. After the desorption experiment, the material was activated with 0.1 mol/L NaOH and used for the next adsorption process. As shown in **Figure 9B**, the adsorption capacities of the adsorbent in the second cycle were a little higher than the initial capacities, suggesting that some adsorption sites can be created during the regeneration process; a similar phenomenon was also found in earlier studies (Zhu et al., 2015). After the second cycle, there was only a subtle decrease in the adsorption capacities for Ce(III) and Gd(III). Furthermore, the prepared porous material maintained relatively high adsorption capacities to Ce(III) and Gd(III) during the whole consecutive adsorption-desorption processes, indicating that the as-prepared hydrogel CMC-g-PAM/ATP exhibited excellent reusability.

CONCLUSION

A convenient, economical, and environmentally friendly strategy was developed for the preparation of interconnected porous adsorbent of CMC-g-PAM/ATP with vegetable oil-in-water Pickering-MIPE templates that was stabilized by raw ATP and a trace amount of T-20. The stability of the emulsion could be easily modulated by the emulsification rate and duration. The type of vegetable oil has no significant influence on either the properties of the emulsion or the porous structure of the material. SEM images indicated that all materials derived via the Pickering-MIPE template method exhibited an excellent interconnected hierarchical porous structure that was not inferior

to that prepared with HIPE. Due to the highly permeable porous structure and abundant functional groups, the materials prepared presented promising potential as excellent adsorbents for the rapid extraction of Ce(III) and Gd(III) from aqueous solution. Furthermore, the materials still exhibited excellent reusability after five consecutive adsorption-desorption processes. This work can be taken as a new contribution to efforts to develop a new pathway to construct porous adsorbents for the adsorption and enrichment of REEs.

DATA AVAILABILITY STATEMENT

All datasets generated for this study are included in the article/supplementary material.

AUTHOR CONTRIBUTIONS

FW contributed to the experimental process and data analysis, wrote the paper, and drew all the figures. YZ contributes to the data analysis and revision of the paper. AW contributed to the experimental design and revision of the paper.

FUNDING

The authors are grateful for financial support from the National Natural Science Foundation of China (21706267), the Major Projects of the National Natural Science Foundation of Gansu, China (18JR4RA001), a Scientific Research Project of Beibu Gulf University, China (17KYQD57), a College Scientific Research Project of the Education department of Guangxi, China (18KY0610), and the Natural Science Fund for Distinguished Young Scholars of Guangxi Province (2017GXNSFFA198007).

REFERENCES

- Ali, O., Osman, H., Sayed, S., and Shalabi, M. (2011). The removal of some rare earth elements from their aqueous solutions on by-pass cement dust (BCD). *J. Hazard. Mater.* 195, 62–67. doi: 10.1016/j.jhazmat.2011.08.014
- Alshameri, A., He, H., Xin, C., Zhu, J., Xinghu, W., Zhu, R., et al. (2019). Understanding the role of natural clay minerals as effective adsorbents and alternative source of rare earth elements: adsorption operative parameters. *Hydrometallurgy* 185, 149–161. doi: 10.1016/j.hydromet.2019.02.016
- Anastopoulos, I., Bhatnagar, A., and Lima, E. C. (2016). Adsorption of rare earth metals: A review of recent literature. *J. Mol. Liq.* 221, 954–962. doi: 10.1016/j.molliq.2016.06.076
- Awual, M. R., Yaita, T., and Shiwaku, H. (2013). Design a novel optical adsorbent for simultaneous ultra-trace cerium(III) detection, sorption and recovery. *Chem. Eng. J.* 228, 327–335. doi: 10.1016/j.cej.2013.05.010
- Babu, C. M., Binnemans, K., and Roosen, J. (2018). EDTA-functionalized activated carbon for the adsorption of rare earths from aqueous solutions. *Ind. Eng. Chem. Res.* 57, 1487–1497. doi: 10.1021/acs.iecr.7b04274
- Chatterjee, S., Lee, M. W., and Woo, S. H. (2009). Influence of impregnation of chitosan beads with cetyl trimethyl ammonium bromide on their structure and adsorption of congo red from aqueous solutions. *Chem. Eng. J.* 155, 254–259. doi: 10.1016/j.cej.2009.07.051
- Chen, H., Sharma, S. K., Sharma, P. R., Yeh, H., Johnson, K., and Hsiao, B. S. (2019). Arsenic(III) removal by nanostructured dialdehyde cellulose-cysteine microscale and nanoscale Fibers. *ACS Omega.* 4, 22008–22020. doi: 10.1021/acs.omega.9b03078
- Chen, W., Wang, L., Zhuo, M., Liu, Y., Wang, Y., and Li, Y. (2014). Facile and highly efficient removal of trace Gd(III) by adsorption of colloidal graphene oxide suspensions sealed in dialysis bag. *J. Hazard. Mater.* 279, 546–553. doi: 10.1016/j.jhazmat.2014.06.075
- Colla, E., do Amaral Sobral, P. J., and Menegalli, F. C. (2006). Amaranthus cruentus flour edible films: influence of stearic acid addition, plasticizer concentration, and emulsion stirring speed on water vapor permeability and mechanical properties. *J. Agr. Food Chem.* 54, 6645–6653. doi: 10.1021/jf0611217
- Delrish, E., Khanchi, A., Outokesh, M., Tayyebi, A., and Tahvildari, K. (2014). Study on the adsorption of samarium and gadolinium ions by a biopolymer microcapsules containing DEHPA/ TOPO extract. *J. Appl. Chem. Res.* 220, 448–455. doi: 10.1016/j.snb.2015.05.101
- Gautier, F., Destribats, M., Perrier-Cornet, R., Dechézelles, J.-F., Giermanska, J., Héroguez, V., et al. (2007). Pickering emulsions with stimutable particles: from highly- to weakly-covered interfaces. *Phys. Chem. Chem. Phys.* 9, 6455–6462. doi: 10.1039/b710226g
- Ghaedi, M., Hajjati, S., Mahmudi, Z., Tyagi, I., Agarwal, S., Maity, A., et al. (2015). Modeling of competitive ultrasonic assisted removal of the dyes-Methylene blue and Safranin-O using Fe_3O_4 nanoparticles. *Chem. Eng. J.* 268, 28–37. doi: 10.1016/j.cej.2014.12.090
- Ghorai, S., Sarkar, A., Raoufi, M., Panda, A. B., Schönherr, H., and Pal, S. (2014). Enhanced removal of methylene blue and methyl violet dyes from aqueous solution using a nanocomposite of hydrolyzed polyacrylamide grafted xanthan gum and incorporated nanosilica. *ACS Appl. Mater. Inter.* 6, 4766–4777. doi: 10.1021/am4055657

- Gładysz-Plaska, A., Majdan, M., and Grabias, E. (2014). Adsorption of La, Eu and Lu on raw and modified red clay. *J. Radioanal. Nucl. Chem.* 301, 33–40. doi: 10.1007/s10967-014-3111-4
- Gudarzi, M. M., and Sharif, F. (2011). Self assembly of graphene oxide at the liquid–liquid interface: a new route to the fabrication of graphene based composites. *Soft Matter* 7, 3432–3440. doi: 10.1039/c0sm01311k
- Gupta, V. K., Nayak, A., Agarwal, S., and Tyagi, I. (2014). Potential of activated carbon from waste rubber tire for the adsorption of phenolics: effect of pre-treatment conditions. *J. Colloid. Interface. Sci.* 417, 420–430. doi: 10.1016/j.jcis.2013.11.067
- Hou, H., Wang, Y., Xu, J., and Chen, J. (2013). Solvent extraction of La(III) with 2-ethylhexyl phosphoric acid-2-ethylhexyl ester (EHEHPA) by membrane dispersion micro-extractor. *J. Rare Earth* 31, 1114–1118. doi: 10.1016/S1002-0721(12)60413-X
- Iftikhar, S., Srivastava, V., and Sillanpää, M. (2017). Synthesis and application of LDH intercalated cellulose nanocomposite for separation of rare earth elements (REEs). *Chem. Eng. J.* 309, 130–139. doi: 10.1016/j.cej.2016.10.028
- Ijagbemi, C. O., Baek, M. H., and Kim, D. S. (2010). Adsorptive performance of un-calcined sodium exchanged and acid modified montmorillonite for Ni²⁺ removal: equilibrium, kinetics, thermodynamics and regeneration studies. *J. Hazard. Mater.* 174, 746–755. doi: 10.1016/j.jhazmat.2009.09.115
- Ikem, V. O., Angelika, M., Horozov, T. S., and Alexander, B. (2010a). Highly permeable macroporous polymers synthesized from pickering medium and high internal phase emulsion templates. *Adv. Mater.* 22, 3588–3592. doi: 10.1002/adma.201000729
- Ikem, V. O., Menner, A., and Bismarck, A. (2008). High Internal Phase Emulsions Stabilized Solely by Functionalized Silica Particles. *Angew. Chem. Int. Ed.* 47, 8277–8279. doi: 10.1002/anie.200802244
- Ikem, V. O., Menner, A., and Bismarck, A. (2010b). High-porosity macroporous polymers synthesized from titania-particle-stabilized medium and high internal phase emulsions. *Langmuir* 26, 8836–8841. doi: 10.1021/la9046066
- Jaya, S. V. C., Das, D., and Das, N. (2014). Optimization of parameters for cerium(III) biosorption onto biowaste materials of animal and plant origin using 5-level Box-Behnken design: Equilibrium, kinetic, thermodynamic and regeneration studies. *J. Rare Earth* 32, 745–757. doi: 10.1016/S1002-0721(14)60136-8
- Jiayi, H., Kaijun, X., Zhongjie, D., Wei, Z., and Chen, Z. (2015). β -Cyclodextrin functionalized polystyrene porous monoliths for separating phenol from wastewater. *Carbohydr. Polym.* 120, 85–91. doi: 10.1016/j.carbpol.2014.12.011
- Klemm, D., Cranston, E. D., Fischer, D., Gama, M., Kedzior, S. A., Kralisch, D., et al. (2018). Nanocellulose as a natural source for groundbreaking applications in materials science: today's state. *Mater. Today* 21, 720–748. doi: 10.1016/j.mattod.2018.02.001
- Klemm, D., Heublein, B., Fink, H. P., and Bohn, A. (2005). Cellulose: fascinating biopolymer and sustainable raw material. *Angew. Chem. Int. Ed.* 44, 3358–3393. doi: 10.1002/anie.200460587
- Liatou, I., Efstathiou, M., and Pashalidis, I. (2015). Adsorption of trivalent lanthanides by marine sediments. *J. Radioanal. Nucl. Chem.* 304, 41–45. doi: 10.1007/s10967-014-3448-8
- Liu, C., Yan, C., Zhou, S., and Ge, W. (2017). Fabrication of sponge biomass adsorbent through UV-induced surface-initiated polymerization for the adsorption of Ce(III) from wastewater. *Water Sci. Technol.* 75:2755. doi: 10.2166/wst.2017.144
- Ma, L., Luo, X., Ning, C., Xue, Y., Zhu, S., Zhen, F., et al. (2014). Facile fabrication of hierarchical porous resins via high internal phase emulsion and polymeric porogen. *Appl. Surf. Sci.* 305, 186–193. doi: 10.1016/j.apsusc.2014.03.036
- Maranescu, B., Lupa, L., and Visa, A. (2019). Synthesis, characterization and rare earth elements adsorption properties of phosphonate metal organic frameworks. *Appl. Surf. Sci.* 481, 83–91. doi: 10.1016/j.apsusc.2019.03.067
- Mittal, A., Mittal, J., Malviya, A., and Gupta, V. K. (2010). Removal and recovery of Chrysoidine Y from aqueous solutions by waste materials. *J. Colloid Interf. Sci.* 344, 497–507. doi: 10.1016/j.jcis.2010.01.007
- Moldoveanu, G. A., and Papangelakis, V. G. (2012). Recovery of rare earth elements adsorbed on clay minerals: I. Desorption mechanism. *Hydrometallurgy* 117–118, 71–78. doi: 10.1016/j.hydromet.2012.02.007
- Mondal, S., Ghar, A., Satpati, A. K., Sinharoy, P., Singh, D. K., Sharma, J. N., et al. (2019). Recovery of rare earth elements from coal fly ash using TEHDGA impregnated resin. *Hydrometallurgy* 185, 93–101. doi: 10.1016/j.hydromet.2019.02.005
- Ogata, T., Narita, H., and Tanaka, M. (2015). Adsorption behavior of rare earth elements on silica gel modified with diglycol amic acid. *Hydrometallurgy* 152, 178–182. doi: 10.1016/j.hydromet.2015.01.005
- Oh, B. H. L., Alexander, B., and Chan-Park, M. B. (2014). High internal phase emulsion templating with self-emulsifying and thermoresponsive chitosan-graft-PNIPAM-graft-oligoproline. *Biomacromolecules* 15, 1777–1787. doi: 10.1021/bm500172u
- Page, M. J., Quinn, J. E., and Soldenhoff, K. H. (2019). The impact of sulfate ions on the ion exchange of rare earth elements. *Hydrometallurgy* 186, 12–20. doi: 10.1016/j.hydromet.2019.03.003
- Rahman, M. L., Biswas, T. K., Sarkar, S. M., Yusoff, M. M., Sarjadi, M. S., Arshad, S. E., et al. (2017). Adsorption of rare earth metals from water using a kenaf cellulose-based poly(hydroxamic acid) ligand. *J. Mol. Liq.* 243, 616–623. doi: 10.1016/j.molliq.2017.08.096
- Rajendran, S., Khan, M. M., Gracia, F., Qin, J., Gupta, V. K., and Arumainathan, S. (2016). Ce³⁺-ion-induced visible-light photocatalytic degradation and electrochemical activity of ZnO/CeO₂ nanocomposite. *Sci Rep.* 6:31641. doi: 10.1038/srep31641
- Ren, H., Gao, Z., Wu, D., Jiang, J., Sun, Y., and Luo, C. (2016). Efficient Pb(II) removal using sodium alginate-carboxymethyl cellulose gel beads: preparation, characterization, and adsorption mechanism. *Carbohydr. Polym.* 137, 402–409. doi: 10.1016/j.carbpol.2015.11.002
- Saravanan, R., Joicy, S., Gupta, V. K., Narayanan, V., and Stephen, A. (2013). Visible light induced degradation of methylene blue using CeO₂/V₂O₅ and CeO₂/CuO catalysts. *Mater. Sci. Eng. C* 33, 4725–4731. doi: 10.1016/j.msec.2013.07.034
- Schirhagl, R. (2014). Bioapplications for molecularly imprinted polymers. *Anal. Chem.* 86, 250–261. doi: 10.1021/ac401251j
- Sharma, P. R., Joshi, R., Sharma, S. K., and Hsiao, B. S. (2017). A simple approach to prepare carboxycellulose nanofibers from untreated biomass. *Biomacromolecules* 18, 2333–2342. doi: 10.1021/acs.biomac.7b00544
- Sullivan, A. P., and Kilpatrick, P. K. (2002). The effects of inorganic solid particles on water and crude oil emulsion stability. *Ind. Eng. Chem. Res.* 41, 3389–3404. doi: 10.1021/ie010927n
- Survey, U. S. G. (2014). *Rare Earths, Mineral Commodity Summaries*, 128–129.
- Voßenkaul, D., Stoltz, N., Meyer, F. M., and Friedrich, B. (2015). “Extraction of rare earth elements from non-chinese ion adsorption clays,” in *European Metallurgical Conference (Düsseldorf)*.
- Wang, F., Wang, W., Zhu, Y., and Wang, A. (2017a). Evaluation of Ce(III) and Gd(III) adsorption from aqueous solution using CTS-g-(AA-co-SS)/ISC hybrid hydrogel adsorbent. *J. Rare Earth* 35, 697–708. doi: 10.1016/S1002-0721(17)60966-9
- Wang, F., Zhu, Y., Wang, W., Zong, L., Lu, T., and Wang, A. (2017b). Fabrication of CMC-g-PAM superporous polymer monoliths via eco-friendly pickering-MIPES for superior adsorption of methyl violet and methylene blue. *Front. Chem.* 5:33. doi: 10.3389/fchem.2017.00033
- Wang, J., Wei, L., Ma, Y., Li, K., Li, M., Yu, Y., et al. (2013). Collagen/cellulose hydrogel beads reconstituted from ionic liquid solution for Cu(II) adsorption. *Carbohydr. Polym.* 98, 736–743. doi: 10.1016/j.carbpol.2013.06.001
- Wang, W., Kang, Y., and Wang, A. (2013). One-step fabrication in aqueous solution of a granular alginate-based hydrogel for fast and efficient removal of heavy metal ions. *J. Polym. Res.* 20, 1–10. doi: 10.1007/s10965-013-0101-0
- Wang, W., Wang, F., Kang, Y., and Wang, A. (2015). Enhanced adsorptive removal of methylene blue from aqueous solution by alkali-activated polygorskite. *Water Air Soil Poll.* 226, 1–13. doi: 10.1007/s11270-015-2355-0
- Xiao, J., Lu, Z., and Li, Y. (2015). Carboxymethylcellulose-supported palladium nanoparticles generated in situ from palladium (II) carboxymethylcellulose: an efficient and reusable catalyst for Suzuki-Miyaura and Mizoroki-Heck reactions. *Ind. Eng. Chem. Res.* 54, 790–797. doi: 10.1021/ie503075d
- Xu, H., Zheng, X., Huang, Y., Wang, H., and Du, Q. (2016). Interconnected porous polymers with tunable pore throat size prepared via pickering high internal phase emulsions. *Langmuir* 32, 38–45. doi: 10.1021/acs.langmuir.5b03037
- Yang, L., Li, C., Wang, D., Li, F., Liu, Y., Zhou, X., et al. (2019). Leaching ion adsorption rare earth by aluminum sulfate for increasing efficiency

- and lowering the environmental impact. *J. Rare Earth*. 37, 429–436. doi: 10.1016/j.jre.2018.08.012
- Yang, P., Mykhaylyk, O. O., Jones, E. R., and Armes, S. P. (2016). RAFT dispersion alternating copolymerization of styrene with *n*-phenylmaleimide: morphology control and application as an aqueous foam stabilizer. *Macromolecules*. 49, 6731–6742. doi: 10.1021/acs.macromol.6b01563
- Yang, T., Wang, L., Mei, L., Yang, C., and Zou, H. (2018). Cross-linked polyvinyl amidoxime fiber: a highly selective and recyclable adsorbent of gallium from Bayer liquor. *Iran. Polym. J.* 27, 1–9. doi: 10.1007/s13726-018-0635-4
- Yantasee, W., Fryxell, G. E., Porter, G. A., Pattamakomsan, K., Sukwarotwat, V., Chouyok, W., et al. (2010). Novel sorbents for removal of gadolinium-based contrast agents in sorbent dialysis and hemoperfusion: preventive approaches to nephrogenic systemic fibrosis. *Nanomed-Nanotechnol.* 6, 1–8. doi: 10.1016/j.nano.2009.05.002
- Ye, H., Zhang, S., Yun, Z., Chu, Y., and Chen, J. (2013). Hydrophilic polymer foams with well-defined open-cell structure prepared from pickering high internal phase emulsions. *J. Polym. Sci. Pol. Chem.*, 51, 2181–2187. doi: 10.1002/pola.26588
- Yi, W., Wu, H., Wang, H., and Du, Q. (2016). Interconnectivity of macroporous hydrogels prepared via graphene oxide-stabilized pickering high internal phase emulsions. *Langmuir* 32, 982–990. doi: 10.1021/acs.langmuir.5b04477
- Zhang, L., Ding, S.-D., Yang, T., Zheng, G.-C. (2009). Adsorption behavior of rare earth elements using polyethyleneglycol (phosphomolybdate and tungstate) heteropolyacid sorbents in nitric solution. *Hydrometallurgy* 99, 109–114. doi: 10.1016/j.hydromet.2009.07.002
- Zhang, Y., Pan, J., Chen, Y., Shi, W., Yan, Y., and Yu, L. (2016). HIPEs template: Towards the synthesis of polymeric catalysts with adjustable porous structure, acid–base strength and wettability for biomass energy conversion. *Chem. Eng. J.* 283, 956–970. doi: 10.1016/j.cej.2015.08.090
- Zhao, F., Repo, E., Meng, Y., Wang, X., Yin, D., and Sillanpää, M. (2016). An EDTA- β -cyclodextrin material for the adsorption of rare earth elements and its application in preconcentration of rare earth elements in seawater. *J. Colloid Interf. Sci.* 465, 215–224. doi: 10.1016/j.jcis.2015.11.069
- Zhao, H., Xia, J., Yin, D., Luo, M., Yan, C., and Du, Y. (2019). Rare earth incorporated electrode materials for advanced energy storage. *Coordin. Chem. Rev.* 390, 32–49. doi: 10.1016/j.ccr.2019.03.011
- Zhou, Q., Yan, C., and Luo, W. (2016). Preparation of a novel carboxylate-rich wheat straw through surface graft modification for efficient separation of Ce(III) from wastewater. *Mater. Design* 97, 195–203. doi: 10.1016/j.matdes.2016.02.081
- Zhou, S., Li, X., Shi, Y., Alshameri, A., and Yan, C. (2014). Preparation, characterization, and Ce(III) adsorption performance of poly(allylamine)/silica composite. *Desalin. Water Treat.* 56, 1–14. doi: 10.1080/19443994.2014.979239
- Zhou, Y., Fu, S., Zhang, L., Zhan, H., and Levit, M. V. (2014). Use of carboxylated cellulose nanofibrils-filled magnetic chitosan hydrogel beads as adsorbents for Pb(II). *Carbohydr. Polym.* 101, 75–82. doi: 10.1016/j.carbpol.2013.08.055
- Zhu, Y., Wang, W., Zheng, Y., Wang, F., and Wang, A. (2016a). Rapid enrichment of rare-earth metals by carboxymethyl cellulose-based open-cellular hydrogel adsorbent from HIPEs template. *Carbohydr. Polym.* 140, 51–58. doi: 10.1016/j.carbpol.2015.12.003
- Zhu, Y., Zheng, Y., and Wang, A. (2015). Preparation of granular hydrogel composite by the redox couple for efficient and fast adsorption of La(III) and Ce(III). *J. Environ. Chem. Eng.* 3, 1416–1425. doi: 10.1016/j.jece.2014.11.028
- Zhu, Y., Zheng, Y., Wang, F., and Wang, A. (2016b). Monolithic supermacroporous hydrogel prepared from high internal phase emulsions (HIPEs) for fast removal of Cu²⁺ and Pb²⁺. *Chem. Eng. J.* 284, 422–430. doi: 10.1016/j.cej.2015.08.157

Conflict of Interest: The authors declare that the research was conducted in the absence of any commercial or financial relationships that could be construed as a potential conflict of interest.

Copyright © 2020 Wang, Zhu and Wang. This is an open-access article distributed under the terms of the Creative Commons Attribution License (CC BY). The use, distribution or reproduction in other forums is permitted, provided the original author(s) and the copyright owner(s) are credited and that the original publication in this journal is cited, in accordance with accepted academic practice. No use, distribution or reproduction is permitted which does not comply with these terms.